Continuous Flow Hyperpolarized ^{129}Xe NMR for Studying Porous Polymers and Blends

Roberto Simonutti, Silvia Bracco, Angiolina Comotti, Michele Mauri, and Piero Sozzani*

Department of Materials Science, University of Milano-Bicocca, INSTM Via R. Cozzi 53, 20125 Milan, Italy

Received March 1, 2006. Revised Manuscript Received May 28, 2006

Hyperpolarized (HP) ^{129}Xe NMR spectroscopy has been applied to high-impact porous polymers and copolymers obtained by the latest generation supported Ziegler−Natta catalysts. Hyperpolarized xenon gas rapidly flows into the open cavities and then penetrates the amorphous phases of polypropylene (PP) and ethylene−propylene copolymer (EPR) millimeter particles. Variable temperature HP ^{129}Xe NMR demonstrated that xenon uptake is largely modulated by the motional state of the phases and is considerably reduced if glass transition is approached because the polymeric matrix becomes impermeable to the gas phase. This is an alternative method to detect the occurrence of the glass transition even in polymeric complex systems. The competitive absorption of xenon in PP and EPR microphases shows the morphology of the particles and the phase architecture. The intermixing of the phases at micrometer level was established on the basis of the xenon diffusion rates. 2D ^{129}Xe EXSY experiments disclose the freshly polarized xenon exchange pathways from the free gas to the EPR phase and, later on, between the polymeric phases.

Introduction

Thermally polarized xenon NMR spectroscopy is a remarkable technique for the study of a diversity of materials. The atom of xenon diffusing in zeolites, clathrates, and clays can describe the accessible cavities and channels and provide information on their size, shape, and chemical nature.[1] Thermally polarized ^{129}Xe NMR has been applied successfully to polymers to determine the chain mobility, the glass-transition temperature, and the free volume of the rubbery amorphous phase.[2] Each polymer shows its own chemical shift that can be used to follow phase separation as well as to measure domain sizes in multiphase blends.[3]

The sensitivity of ^{129}Xe NMR can be enhanced by orders of magnitude by hyperpolarization (HP) that, exploiting optical pumping spin-exchange,[4] produces a significant xenon signal after a few scans. Considerable improvement of the technique has been achieved by the development of continuous flow (CF) apparatus, that can continuously supply hyperpolarized xenon to the sample inside the NMR coil.[5] Recently, an intense activity has been focused on the applications of HP ^{129}Xe NMR to studies of single microcrystals, host−guest complexes, fullerenes, material surfaces, and thin films.[6] HP Xe NMR has been applied to the study of porous polymers with particular attention to the surface adsorption, the description of micro- and mesoporosity, and the determination of surface-to-volume ratio.[7−9]

* Author to whom correspondence should be addressed. E-mail: piero.sozzani@mater.unimib.it.

(1) (a) Ito, T.; Fraissard, J. *J. Chem. Phys.* **1982**, *76*, 5225−5229. (b) Ripmeester, J. A. *J. Am. Chem. Soc.* **1982**, *104*, 289−290. (c) Miller, K. W.; Reo, N. V.; Schoot Uiterkamp, A. J. M.; Stengle, D. P.; Stengle, T. R.; Williamson, K. L. *Proc. Natl. Acad. Sci. U.S.A.* **1981**, *78*, 4946−4949. (d) Dybowski, C.; Bansal, N.; Duncan, T. M. *Annu. Rev. Phys. Chem.* **1991**, *42*, 433−464. (e) Barrie, P. J.; Klinowski, J. *Prog. Nucl. Magn. Reson. Spectrosc.* **1992**, *24*, 91−108. (f) Jokisaari, J. *Prog. Nucl. Magn. Reson. Spectrosc.* **1994**, *26*, 1−26. (g) Raftery, D.; Chmelka, B. F. In *NMR Basic Principles and Progress;* Diehl, P., Fluck, E., Gunther, H., Kosfeld, R., Seelig, J. Eds.; Springer-Verlag: Berlin, 1994; Vol. 30, pp 111−158. (h) Ratcliffe, C. I. *Annu. Rep. NMR Spectrosc.* **1998**, *36*, 124−208. (i) Springuel-Huet, M. A.; Bonardet, J. L.; Gedeon, A.; Fraissard, J. *Magn. Reson. Chem.* **1999**, *37*, S1−S13.

(2) (a) Stengle, T. R.; Williamson, K. *Macromolecules* **1987**, *20*, 1428−1430. (b) Brownstein, S. K.; Roovers, J. E. L.; Worsfold, D. J. *Magn. Reson. Chem.* **1988**, *26*, 392−393. (c) Kennedy, G. J. *Polym. Bull.* **1990**, *23*, 605−608. (d) Kentgens, A. P. M.; Van Boxtel, H. A.; Verweel, R.-J.; Veeman, W. S. *Macromolecules* **1991**, *24*, 3712−3714. (e) Miller, J. B.; Walton, J. H.; Roland, C. M. *Macromolecules* **1993**, *26*, 5602−5610. (f) Morgan, D. R.; Stejskal, E. O.; Andrady, A. L. *Macromolecules* **1999**, *32*, 1897−1903. (g) Menge, H.; Kühn, H.; Blümich, B.; Blümler, P.; Schneider, H. *Macromol. Mater. Eng.* **2000**, *282*, 1−4. (h) Merkel, T. C.; Toy, L. G.; Andrady, A. L.; Gracz, H.; Stejskal, E. O. *Macromolecules* **2003**, *36*, 353−358.

(3) (a) Walton, J. H.; Miller, J. B.; Roland, C. M. *J. Polym. Sci., Part B: Polym. Phys.* **1992**, *30*, 527−532. (b) Walton, J. H.; Miller, J. B.; Roland, C. M.; Nagode, J. B. *Macromolecules* **1993**, *26*, 4052−4054. (c) Tomaselli, M.; Meier, B. H.; Robyr, P.; Suter, U. W.; Ernst, R. R. *Chem. Phys. Lett.* **1993**, *205*, 145−152. (d) Mansfeld, M.; Veeman, W. S. *Chem. Phys. Lett.* **1994**, *222*, 422−424. (e) Miyoshi, T.; Takegoshi, K.; Terao, T. *Polymer* **1997**, *38*, 5475−5480. (f) Schantz, S.; Veeman, W. S. *J. Polym. Sci., Part B: Polym. Phys.* **1997**, *35*, 2681−2688. (g) Yang, C.; Wen, W. Y.; Jones, A. A.; Inglefield, P. T. *Solid State Nucl. Magn. Reson.* **1998**, *12*, 153−164.

(4) (a) Raftery, D.; Long, H.; Meersmann, T.; Grandinetti, P. J.; Reven, L.; Pines, A. *Phys. Rev. Lett.* **1991**, *66*, 584−587. (b) Song, Y.; Goodson, B. M.; Pines, A. *Spectroscopy* **1999**, *14*, 26−33. (c) Goodson, B. M. *J. Magn. Reson.* **2002**, *155*, 157−216.

(5) (a) Haake, M.; Pines, A.; Reimer, J. A.; Seydoux, R. *J. Am. Chem. Soc.* **1997**, *119*, 11711−11712. (b) Seydoux, R.; Pines, A.; Haake, M.; Reimer, J. A. *J. Phys Chem. B* **1999**, *103*, 4629−4637. (c) Brunner, E.; Haake, M.; Pines, A.; Reimer, J. A.; Seydoux, R. *Chem. Phys. Lett.* **1998**, *290*, 112−116. (d) Moudrakovski, I. L.; Nossov, A.; Lang, S.; Breeze, S. R.; Ratcliffe, C. I.; Simard, B.; Santyr, G.; Ripmeester, J. A. *Chem. Mater.* **2000**, *12*, 1181−1183. (e) Nossov, A.; Haddad, E.; Guenneau, F.; Mignon, C.; Gedeon, A.; Grosso, D.; Babonneau, F.; Bonhomme, C.; Sanchez, C. *Chem. Commun.* **2002**, *21*, 2476−2477.

10.1021/cm060499h CCC: $33.50
Published on Web 08/19/2006

Here, we propose CF−HP ^{129}Xe NMR as an effective technique for the characterization of porous polymeric materials with xenon dissolving in the solid phase and collecting information about the phase transitions and blending of the polymers. In this paper, we report the application of CF−HP ^{129}Xe NMR to the study of polyolefines polymerized by the latest generation of supported Ziegler−Natta catalysts.[10] This technique allowed us to address several important parameters in polymer particles such as glass transition and phase architecture. By the Ziegler−Natta supported-catalyst system, it is possible to obtain millimeter-sized polymer particles that reproduce the spherical morphology of the original catalyst grain.[11,12] The polymer grown within the catalyst particles creates a porous network accessible to diffusing xenon that permeates the rubbery amorphous phases of the polymeric material. The porous particles can be used as the reaction support for a second polymerization with a different monomer or a monomer mixture producing an intimate polymer alloy, interesting for important industrial applications. In the final material, HP ^{129}Xe NMR spectroscopy can recognize the single phases and their intimacy.

Experimental Section

Continuous Flow Hyperpolarized ^{129}Xe NMR. A sketch of the home-built apparatus for the production of a continuous flow of HP xenon is reported in Figure 1. The pumping cell is located in the fringe magnetic field (50 G) of the superconducting wide bore NMR magnet (7.04 T). A fiber coupled diode array laser (Coherent FAP-System) delivering 16 W at 795 nm was used to excite rubidium. Circular polarization of the light was achieved using a beam splitting cube (Thorlabs) and quarter-wave plate (CVI). The pumping cell, containing rubidium and a mixture of 2% xenon, 2% nitrogen, and 96% helium at 4 atm, was heated at 448 K. The circularly polarized laser light collimated to the cell pumps the Rb electronic levels. In the cell, collisions between Rb and Xe promoted the exchange of polarization in favor of the nuclear spin levels of xenon. Hyperpolarized Xe was then allowed to flow at ambient pressure over the sample inside the NMR coil via Teflon tubing (Swagelok). Gas flow rates were optimized to highest signal intensity, typically 300 cm^3/min. The polarization was higher than 4.5%, with an enhancement factor of more than 7000 over thermally polarized gas, as calculated by comparison with a sealed sample of pure xenon at 1.5 atm (84.4% ^{129}Xe isotope).[13] Therefore, the contribution of thermally polarized Xe is negligible in the experiments, its signal being at least 3 orders of magnitude smaller than the hyperpolarized one. No dependence of the signal intensity on the time of exposure to the xenon stream has been observed. The samples have been exposed to the xenon stream for at least 15 min before starting the NMR experiments. NMR experiments were carried out on a Bruker Avance 300 spectrometer operating at Larmor Frequency of 83.02 MHz for ^{129}Xe.

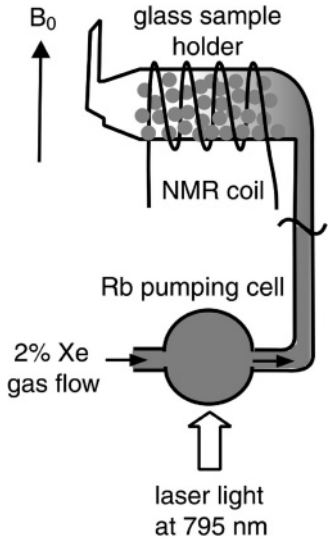

Figure 1. Scheme of CF−HP ^{129}Xe NMR apparatus; the components are not represented on the same scale. A fiber coupled diode array laser delivers light at 795 nm onto the polarizer; after passing through $\lambda/4$ lenses, the light becomes circularly polarized and is used for the excitation of rubidium in the pumping cell. In the cell, filled by a mixture of Xe/N_2/He, collisions between Rb and Xe promote an exchange of polarization in favor of the nuclear spin levels of xenon. Hyperpolarized Xe flows via Teflon tubing over the sample inside the NMR coil.

A tube constitutes the sample holder; two filters are placed at the extremities, and one acts as the inlet for the xenon stream and the other acts as the outlet. Attention was always paid to fill completely the sample holder to keep the intergranule void spaces as constant as possible. A typical $\pi/2$ pulse duration was 7 μs. Typically, the spectra were recorded with 128 scans and 500 ms of recycle delay. Variable temperatures were achieved by flowing cooled or heated nitrogen gas around the sample region. Two-dimensional (2D) exchange NMR is a powerful technique to investigate slow dynamic processes occurring on a time-scale up to several seconds.[13] The 2D exchange experiments were run with 1.2-s recycle delay and spectral width of 29 kHz in both t_1 and t_2 dimensions. There were 128 t_1 increments. 2D data were collected in TPPI mode. Mixing times were varied from 50 to 500 ms.

(6) (a) Terskikh, V. V.; Moudrakovski, I. L.; Du, H.; Ratcliffe, C. I.; Ripmeester, J. A. *J. Am. Chem. Soc.* **2001**, *123*, 10399−10400. (b) Sozzani, P.; Comotti, A.; Simonutti, R.; Meersmann, T.; Logan, J. W.; Pines, A. *Angew. Chem., Int. Ed.* **2000**, *39*, 2695−2698. (c) Anala, S.; Pavlovskaya, G. E.; Pichumani, P.; Dieken, T. J.; Olsen, M. D.; Meersmann, T. *J. Am. Chem. Soc.* **2003,** *125*, 13298−13302. (d) Jansch, H. J.; Gerhard, P.; Koch, M. *Proc. Natl. Acad. Sci.* **2004**, *101*, 14715−13719. (e) Meersmann, T.; Logan, J. W.; Simonutti, R.; Caldarelli, S.; Comotti, A.; Sozzani, P.; Kaiser, L. G.; Pines, A. *J. Phys. Chem. A* **2000**, *104*, 11665−11670. (f) Kneller, J. M.; Soto, R. J.; Surber, S. E.; Colomer, J.-F.; Fonseca, A.; Nagy, J. B.; Van Tendeloo, G.; Pietrass, T. *J. Am. Chem. Soc.* **2000**, *122*, 10591−10597.
(7) (a) Raftery, D.; Reven, L.; Long, H.; Pines, A.; Tang, P.; Reimer, J. A. *J. Phys. Chem.* **1993**, *97*, 1649−1655. (b) Long, H. W.; Gaede, H. C.; Shore, J.; Reven, L.; Bowers, C. R.; Kritzenberger, J.; Pietrass, T.; Pines, A.; Tang, P.; Reimer, J. A. *J. Am. Chem. Soc.* **1993**, *115*, 8491−8492.
(8) Butler, J. P.; Mair, R. W.; Hoffmann, D.; Hrovat, M. I.; Rogers, R. A.; Topulos, G. P.; Walsworth, R. L.; Patz, S. *J. Phys.: Condens. Matter* **2002**, *14*, L297−L304.
(9) (a) Moudrakovski, I. L.; Wang, L.-Q.; Baumann, T.; Satcher, J. H.; Exarhos, G. J.; Ratcliffe, C. I.; Ripmeester, J. A. *J. Am. Chem. Soc.* **2004**, *126*, 5052−5053. (b) Moudrakovski, I. L.; Ratcliffe, C. I.; Ripmeester, J. A.; Wang, L.-Q.; Exarhos, G. J.; Baumann, T. F.; Satcher, J. H. *J. Phys. Chem. B* **2005**, *109*, 11215−11222.
(10) (a) Mülhaupt, R. *Macromol. Chem. Phys.* **2003**, *204*, 289−327. (b) Böhm, L. L. *Angew. Chem., Int. Ed.* **2003**, *42*, 5010−5030. (c) Severn, J. R.; Chadwick, J. C.; Duchateau, R.; Friederichs, N. *Chem. Rev.* **2005** *105*, 4073−4147.
(11) (a) Cecchin, G.; Morini, G.; Pelliconi, A. *Macromol. Symp.* **2001**, *173*, 195−209. (b) Cecchin, G.; Marchetti, E.; Baruzzi, G. *Macromol. Chem. Phys.* **2001**, *202*, 1987−1994. (c) Pater, J. T. M.; Weickert, G.; van Swaaij, W. P. M. *J. Appl. Polym. Sci.* **2003**, *87*, 1421−1431. (d) Urdampilleta, I.; Gonzalez, A.; Iruin, J. J.; de la Cal, J. C.; Asua, J. M. *Macromolecules* **2005**, *38*, 2795−2801.
(12) Noristi, L.; Marchetti, E.; Baruzzi, G.; Sgarzi, P. *J. Polym Sci., Part A: Polym. Chem.* **1994**, *32*, 3047−3059.
(13) (a) Zook, A. L.; Adhyaru, B. B.; Bowers, C. R. *J. Magn. Res.* **2002**, *159*, 175−182. (b) Jeener, J.; Meier, B. H.; Bachmann, P.; Ernst, R. R. *J. Chem. Phys.* **1979**, *71*, 4546−4553.

Table 1. Analytical Data and Thermal Properties of PP Based Granule

sample[a]	PP/EPR (wt %)	ethyl. in EPR[b] (mol %)	mp PP[c] (°C)	ΔH tot[c] (J/g)	ΔH PP[d] (J/g)	T_g[c] (K)	average diameter (mm)
PP	100/0	0	164	−84.1	−84.1	260	2.2
PP/EPR-47-L	53/47	33	162	−67.9	−44.1	n.d.	2.6
PP/EPR-68-L	32/68	38	164	−43.1	−27.4	236	3.6
PP/EPR-67-H	33/67	72	164	−52.7	−28.3	220	3.7

[a] In the PP/EPR samples, the number represents the fraction of EPR and H and L letters indicate high and low ethylene content, respectively. [b] As determined from ^{13}C NMR spectra. [c] Data obtained by differential scanning calorimeter. [d] Enthalpy due to the PP fraction.

Materials and Characterization. Isotactic polypropylene (PP) and polypropylene/ethylene−propylene rubber (PP/EPR) millimeter particles, produced by high-activity $MgCl_2/TiCl_4$ supported Ziegler−Natta catalysts and prepared in the presence of a 1,3 diether as Lewis base, were provided by BASELL. Sample composition determined by ^{13}C MAS NMR and calorimetric analysis is described below. The photographical images of the particles, X-ray diffraction patterns, ^{13}C MAS NMR spectra, and Differential Scanning Calorimetry (DSC) characterization of the samples are reported in the Supporting Information. Mercury porosimetry data show a surface area ranging from 10 to 15 m^2/g. X-ray diffraction analysis of the samples shows the presence of crystalline isotactic polypropylene in the α form in agreement with the ^{13}C MAS NMR spectra (Supporting Information).[14]

Results and Discussion

The spherical polymer samples are constituted by either pure polypropylene PP or by PP with a varied amount of ethylene/propylene EPR rubber grown within the pristine particles of pure polypropylene phase (Table 1). The ethylene fraction in EPR copolymer phase is systematically increased in the series of samples. Calorimetric data and the average diameter of the particle spheres are also reported.

CF−HP ^{129}Xe NMR spectra of PP particles, as-polymerized and after thermal treatment at 140−160 °C, are depicted in Figure 2. Xenon absorbed in the polymeric amorphous phase shows a chemical shift of 222 ppm, in agreement with the literature data[15] and our own observations of thermally polarized Xe NMR for the bulk amorphous phase of isotactic polypropylene. The chemical shift value of 222 ppm demonstrates that xenon resides for a long time (on the NMR time scale) in the amorphous phase and not in restricted empty cavities as typically achieved in porous polymers with a rigid matrix.[9] Spectra with high signal-to-noise ratio are obtained after a few scans. The normalized signal area is reduced progressively as a function of the thermal treatment of the polymer particles. The peak area due to the xenon dissolved in the particles treated at 140 °C is reduced to one-half of that of the pristine sample, and the complete disappearance of the signal occurs after heating the sample at 160 °C (Figure 2d).

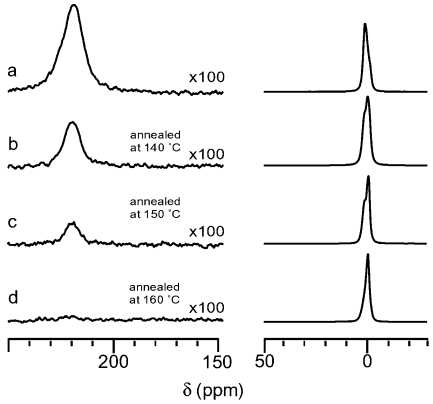

Figure 2. CF−HP ^{129}Xe NMR spectra of Xe gas flowing on (a) as-polymerized PP particles (integral of the PP peak/integral of the gas peak $I_{PP}/I_{gas}(\%) = 5.7$); (b) PP particles heated at 140 °C for 15 min (I_{PP}/I_{gas} (%) = 2.9); (c) PP particles heated at 150 °C for 15 min (I_{PP}/I_{gas} (%) = 1.3); (d) PP particles heated at 160 °C for 15 min. The heights of the gas peaks are the same in all the spectra. The spectra are recorded under a xenon flow of about 0.4 L/h.

This behavior can be explained considering the high surface area of the pristine particles and the reduction of the surface-to-volume ratio obtained by thermal treatment. The peak area depends on the amount of xenon diffusing from the gas phase into the polymer during the recycle delay time, since each pulse excites only the new freshly hyperpolarized xenon. Thus, the relative amount of dissolved xenon with respect to the gas phase is determined by the xenon diffusion coefficient in the bulk, the xenon partition coefficient between the gas phase and the polymer phase, and the recycle delay. Applying the Einstein equation for diffusion[16] $\langle x^2 \rangle = 6D\tau$ and considering the xenon self-diffusion coefficient of about 10^{-12} m^2/s, determined for xenon dissolved in amorphous PP,[17] and a typical recycle delay of 0.5 s, the average distance traveled by a Xe atom in the bulk PP is a few hundred nanometers. During the recycle delay, xenon gas can rapidly invade the accessible pores of the millimeter-size particles because of the open porosity and then can penetrate the amorphous phase of polymeric materials through the extended surface (Figure 3).[18] The process of diffusion through the amorphous phase is slower and is the limiting step; in fact, after sufficiently short times, xenon can diffuse only in that part of the material that is more close to the accessible surface. Thus, only particles with a high surface-to-volume ratio can give rise to an intense signal of dissolved xenon, as the untreated PP samples are. The thermal annealing of the particles at 140 °C causes a partial collapse of the porous structure[18] with a decrease of the surface-to-volume ratio together with an increase of the crystalline fraction, in agreement with the increase of melting enthalpy from 84 to 116 J/g as measured by DSC runs (Supporting Information). The treatment at higher temperature (160 °C) leads to the collapse of the pristine architecture and produces dense and highly crystalline particles with a limited surface area as conventional isotactic polypropylene.

(14) (a) Bracco, S.; Comotti, A.; Simonutti, R.; Camerati, I.; Sozzani, P. *Macromolecules* **2002**, *35*, 1677−1684. (b) Comotti, A.; Simonutti, R.; Bracco, S.; Castellani, L.; Sozzani, P. *Macromolecules* **2001**, *34*, 4879.
(15) (a) Mirabella, F. M.; McFaddin, D. C. *Polymer* **1996**, *37*, 931−938. (b) Mansfeld, M.; Flohr, A.; Veeman, W. S. *Appl. Magn. Reson.* **1995**, *8*, 573−586.
(16) Kärger, J.; Ruthven, D. M. *Diffusion in Zeolites and Other Microporous Solids*; John Wiley and Sons: New York, 1992.
(17) Junker, F.; Veeman, W. S. *Macromolecules* **1998**, *31*, 7010−7013.
(18) (a) Hutchinson, R. A.; Chen, C. M.; Ray, W. H. *J. Appl. Sci.* **1992**, *44*, 1389−1414. (b) Kanellopoulos, V.; Dompazis, G.; Gustafsson, B.; Kiparissides, C. *Ind. Eng. Chem. Res.* **2004**, *43*, 5166−5180.

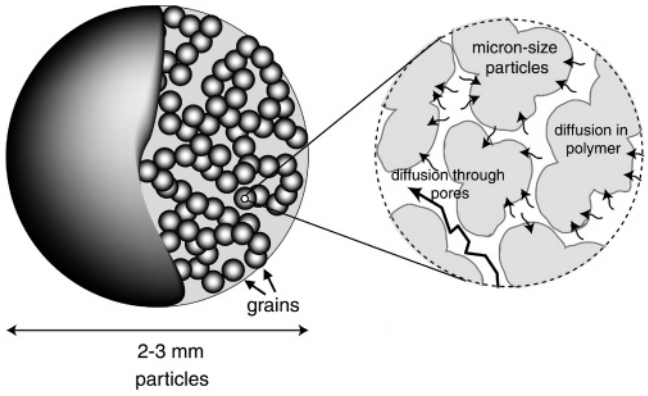

Figure 3. Schematic representation of the multigrain morphology of the polypropylene millimeter particle. The grains are about 100−200 μm in size. The diffusion of xenon inside the grains can proceed via two pathways: first, rapid diffusion through the pores and, second, inside the polymeric amorphous phase of the micrometer-size particles.

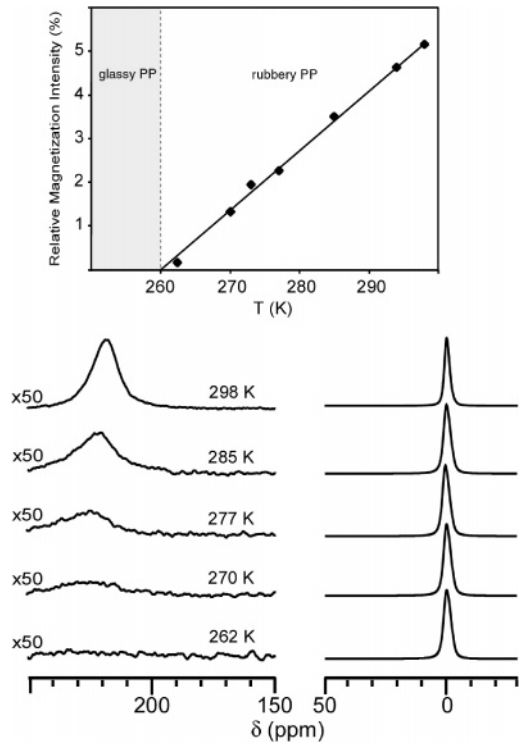

Figure 4. CF−HP ^{129}Xe NMR spectra of Xe gas flowing on PP particles recorded at the reported temperatures. At the top, the ratios of signal intensities (peak areas) of xenon dissolved in PP and the gas phase are reported as a function of temperature.

This final state shows a very weak signal. Thus, the peak area of xenon dissolved in PP spheres is an indication of the high surface area and morphology of the polymer millimeter spheres. This is a demonstration of the dependence of HP xenon NMR signal intensity, under continuous flow mode, on the surface area of a polymeric material. Moreover, the gas xenon chemical shift is influenced by the exchange with the adsorbed xenon on the surface when the surface area is sufficiently high, as in the pristine sample, resonating at 2 ppm. The reduction of the surface area, after the thermal annealing, makes negligible the contribution of the adsorbed xenon to the chemical shift (xenon resonance at 0 ppm).

Variable temperature HP ^{129}Xe NMR spectra of xenon flowing in PP particles are depicted in Figure 4. Reporting the signal intensity (peak area) as a function of the temperature, a linear dependence is observed and we can extrapolate a limit temperature of 260 K at which xenon cannot diffuse appreciably (Figure 4 above). This temperature corresponds to the glass-transition value (T_g) of polypropylene. In fact, at the T_g the permeability of xenon in the glass phase is so low to prevent the recording of a signal from the polymer, notwithstanding the high sensitivity of the HP technique. However, this technique allowed us to record the xenon diffusing into the amorphous phase just a few degrees above the T_g, where xenon penetrates only the very skin of the polymer material since the diffusivity of xenon is slow when polymer chains experience slow motional regimes. This is an alternative way to determine the glass-transition temperature by Xe NMR.[2a,d,e] Other conventional NMR techniques, such as carbon and deuterium NMR, do not recognize the glass transition because they are responsive to high-frequency motional regimes.[19,20]

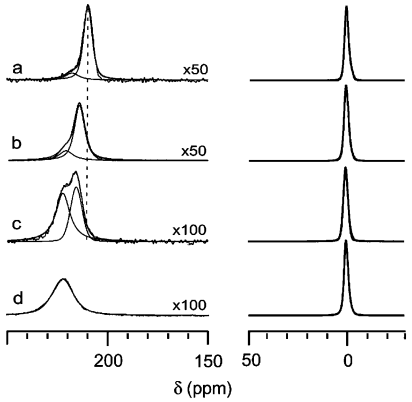

Figure 5. Room-temperature CF−HP ^{129}Xe NMR spectra of Xe gas flowing on (a) PP/EPR-67-H, (b) PP/EPR-68-L, (c) PP/EPR-47-L, and (d) PP particles. Deconvolutions considering one resonance for PP (downfield) and one for EPR (upfield) are also reported.

CF−HP ^{129}Xe NMR spectra on polypropylene/ethylene−propylene PP/EPR particles with variable PP/EPR ratio and ethylene content in the EPR copolymer are reported in Figure 5. The resonance peak of xenon dissolved in polypropylene can be recognized at about 220 ppm. The chemical shift of the upfield signal corresponds to that of xenon in the ethylene−propylene copolymers as observed by thermally polarized xenon NMR.[15] A single resonance for the EPR phase indicates the presence of a homogeneous phase. The signals for xenon in the EPR phase (Figure 5a−c) show the chemical shift strongly dependent on the ethylene content in the rubber (see Table S1 in Supporting Information). As the ethylene fraction in the copolymer increases, the resonance of xenon in the rubbery phase shifts upfield[15] (from 215.7 to 209.6 ppm) and the line width of the signal becomes narrower, indicating the higher EPR mobility (Supporting Information).[14a] The chemical shifts versus compositions are consistent with HP Xe NMR spectra of pure EPR samples, as presented in Supporting Information. Since a resonance is present for each phase, diffusion is not sufficiently rapid to allow xenon atoms to explore both phases within the observation time scale and to produce a coalesced line.

(19) McGrath, K. J.; Ngai, K. L.; Roland, C. M. *Macromolecules* **1992**, *25*, 4911−4914.
(20) White, J. L.; Dias, A. J.; Ashbaugh, J. R. *Macromolecules* **1998**, *31*, 1880−1888.

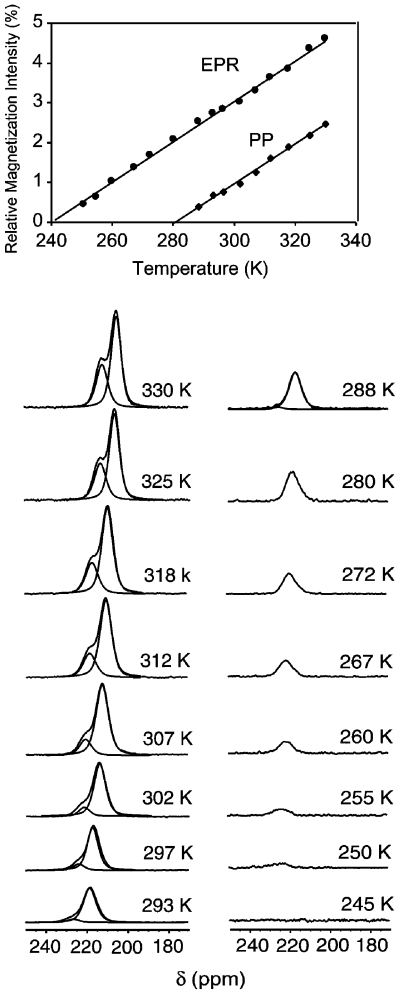

Figure 6. CF−HP ^{129}Xe NMR spectra of PP/EPR-68-L particles recorded at the reported temperatures. The signals at room temperature at about 220 and 214 ppm correspond to the PP and EPR phases, respectively. Temperature dependence of the magnetization intensities (peak areas) with respect to the gas phase (above).

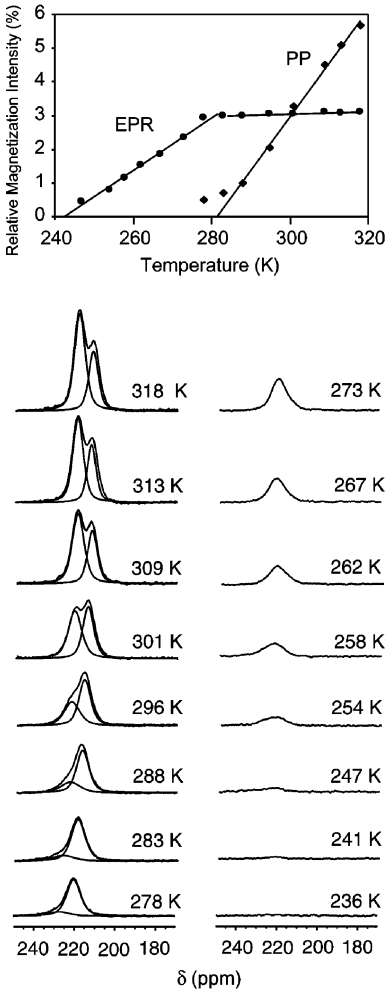

Figure 7. CF−HP ^{129}Xe NMR spectra of PP/EPR-47-L particles recorded at the reported temperatures. The signals at room temperature at about 220 and 216 ppm correspond to the PP and EPR phases, respectively. Temperature dependence of the magnetization intensities (peak areas) with respect to the gas phase (above).

The time τ determined in the fast exchange limit $\tau \cdot (\Delta\omega) \leq 1$ (where $\Delta\omega$ is the difference of the xenon chemical shifts in the pure components) is evaluated as 2 ms. Taking into account this time for diffusion and the Einstein equation ($D \cong 10^{-9}$ m^2/s),[15b] we can evaluate that the PP and EPR phases should, on the average, have dimensions larger than 200 nm. To demonstrate that the structure on a microscopic scale corresponds to the structure on a larger scale (on the millimeter scale), the PP/EPR millimeter spheres were ground under liquid nitrogen. In fact, CF−HP ^{129}Xe NMR spectra of the powders are the same as those recorded on the intact spheres. In the samples with high EPR content, the intensity of the EPR signal largely prevails and the PP signal appears underestimated (Figure 5a and b). This is due to the intrinsic higher permeability of EPR than PP to xenon diffusion at room temperature, which is confirmed by a comparison with thermally polarized xenon NMR responses in PP/EPR blends and impact PP particles.[15]

The samples PP/EPR-68-L and PP/EPR-47-L, containing a similar kind of EPR rubber with a low content of ethylene, were studied by variable temperature measurements (Figures 6 and 7). The two samples allowed us to follow separately the dependence of signal intensities on temperature. In both samples, the disappearance of the EPR signals (214 and 216 ppm at room temperature, respectively) occurs at the extrapolated temperature of 240 K. In the PP/EPR-68-L sample, this temperature is just above the glass-transition temperature of 236 K, as shown by the DSC trace (Supporting Information). Instead, the DSC run of the PP/EPR-47-L sample cannot show any defined glass transition in the temperature range 200−300 K, thus hyperpolarized xenon NMR was shown to be an unusual tool to recognize the motional behavior in the polymers even in the presence of complex mixtures and blends. Owing to the high resolution of the spectra, we could independently analyze the decrease of polypropylene signals that evolve rapidly from high to low temperatures pointing to the temperature of 280 K for both samples (Figures 6 and 7, above). This is due to the stiffening of polypropylene domains that become impermeable to xenon. However, a minor component persists even at lower temperature and is detectable down to the glass transition of amorphous polypropylene as previously discussed. At high temperature, a larger amount of amorphous PP and EPR phases are penetrated by xenon because they are far above the glass-transition temperature. ^{13}C MAS NMR spectra confirm the presence, at room temperature, of mobile

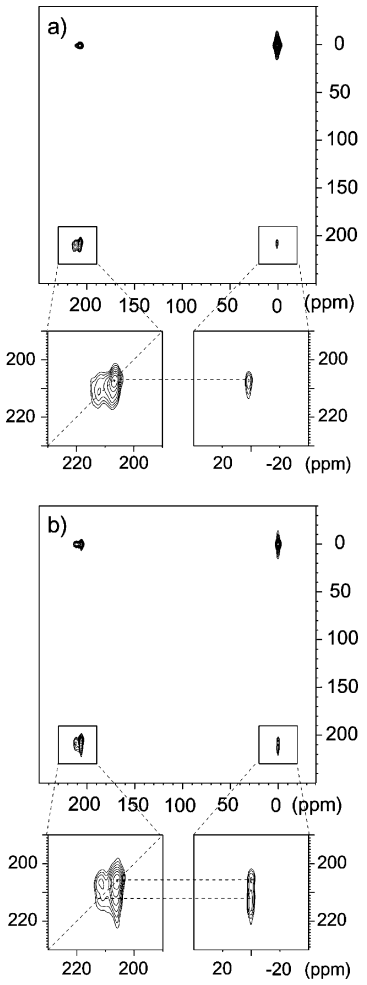

Figure 8. 2D ^{129}Xe EXSY NMR spectra of hyperpolarized xenon at 330 K flowing on sample PP/EPR-68-L with mixing times of (a) 200 ms and (b) 400 ms. Enlargements of relevant regions are reported below the full spectra.

amorphous PP and EPR phases.[14a] In the sample with a comparable amount of PP and EPR phases (PP/EPR-47-L), the response of hyperpolarized xenon dissolved in the EPR phase shows a constant value at high temperatures because a considerable amount of hyperpolarized xenon diffuses out toward the PP phase, as shown below by 2D EXSY NMR experiments. The chemical shift is linearly dependent on the temperature with a slope of 0.2 ppm/K (Supporting Information), in agreement with thermally polarized observations in bulk rubbery polymers.[15b] This result is consistent with a more severe confinement of xenon atoms exerted by the surrounding polymer chains at lower temperature.

For a better understanding of the diffusion phenomena in the two phases and the sequential order of the accessibility of the two phases to the gas phase, 2D exchange NMR experiments (EXSY),[13b] exploiting hyperpolarized xenon, have been performed. 2D EXSY ^{129}Xe spectra recorded at 300 K and 330 K of the PP/EPR-47-L and PP/EPR-68-L samples, respectively, show enough resolution to detect separately, along the diagonal, xenon signals of PP and EPR phases. In Figure 8, the 2D EXSY ^{129}Xe spectra of the PP/EPR-68-L sample are reported at mixing times of 200 and 400 ms. At 200-ms mixing time, the intensity of the diagonal peaks indicates that xenon resides in each phase for a comparable time and intense cross-peaks are shown because of the exchange between the gas signal at 0 ppm and xenon in the EPR phase (Figure 8a, see enlargement). No exchange of xenon can be observed between the gas phase and xenon dissolved in PP indicating that the PP phase is not reached by the gas phase on this time scale. Interestingly, intense cross-peaks are observed for xenon in fast exchange, in the time of 200 ms, between the EPR and the PP phases demonstrating that the two phases are contiguous and blended within a few micrometers.

The cross-peak distribution brings to the deduction that the EPR phase polymerized on the porous polypropylene largely covers the pristine PP phase preventing the direct access of the xenon gas to the PP phase. In fact, PP phase is fed by freshly hyperpolarized xenon through the EPR phase. In other terms, EPR phases occlude the percolation ways to PP phases. At mixing times of 400 ms, the xenon exchange from the EPR to the PP phases intensifies and, in addition, freshly hyperpolarized xenon exchanges with xenon in the PP phase (Figure 8b, see enlargement). A similar behavior is observed for the PP/EPR-47-L already at 300 K (Supporting Information), but at longer mixing times of 500 ms the diagonal peaks are markedly unbalanced in favor of xenon in the PP phase, in agreement with the minor amount of EPR in the PP/EPR-47-L sample compared to the PP/EPR-68-L. By this way, we have identified a path for xenon that sequentially explores the EPR phase and, later on, the PP phase demonstrating the hierarchical structure of the phases in the particles.[9] Our results are consistent with independent observations obtained by microscopies (SEM, TEM, and AFM):[11] at higher degree of copolymerization, the EPR phase surrounds the micrometer-scale particles and fills the interparticle space.

Higher resolution in the HP ^{129}Xe NMR spectra is obtained in samples constituted by PP and EPR with a higher ethylene content (57%). In Figure 9, the 2D EXSY ^{129}Xe spectra at two mixing times of the polymer samples are reported. Along the diagonal, three peaks are present: the free gas, the xenon dissolved in the EPR phase, and the xenon dissolved in the PP phase. For a mixing time of 100 ms, no exchange of xenon can be observed between the polymer phases.

At a longer mixing time, the intensity of the cross-peaks increases and becomes comparable to that of the diagonal peaks that belong to xenon residing in each phase. Interestingly, the cross-peak indicates that, in the time of 500 ms, xenon can exchange between the PP and EPR polymeric phases demonstrating their intimacy. In the polymer particle, at short mixing times, the diagonal peak due to xenon dissolved in EPR is clearly larger than that of xenon in PP, indicating that EPR is more accessible to xenon. The opposite happens at longer mixing times: the diagonal PP peak becomes larger than that of EPR, showing that the diffusion into the PP phase is slower but the residence time is longer. Conventionally, 2D EXSY experiments are carried out on systems in equilibrium conditions and are characterized by back and forward exchange rates of an identical value.[13b] On the contrary, in the "continuous flow" conditions xenon magnetization is in a nonequilibrium state and, depending on the partition coefficients and morphology, it is possible

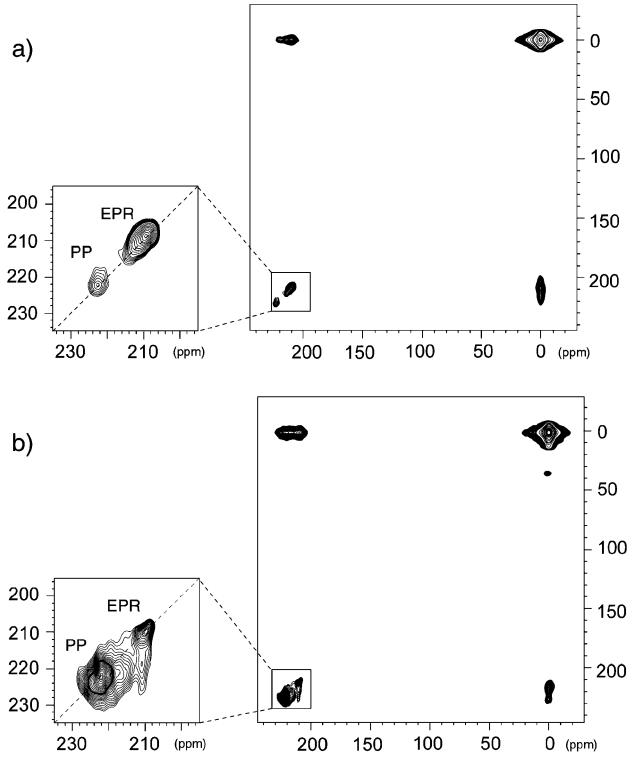

Figure 9. 2D exchange spectra of hyperpolarized xenon flowing on a particle constituted by PP and EPR (57% ethylene). (a) Mixing time of 100 ms, (b) mixing time of 500 ms.

to have a unidirectional diffusion process. For instance, we can consider a system constituted by two domains A and B with A more exposed to the gas phase. At the beginning, xenon enters and diffuses in A and, after a certain time, it reaches B but since xenon concentration is much higher in the former than in the latter, the retrodiffusion is negligible.[5c] This means that at short mixing times the cross-peaks appear unbalanced. The presence of a stronger cross-peak on one side of the diagonal between PP and EPR peaks confirms that, in 500 ms, xenon can enter the EPR phase and then diffuses to the PP one, but the reverse trajectory is considerably less probable.

Conclusions

Hyperpolarized ^{129}Xe NMR spectroscopy was applied to the study of rubbery polymers and blends providing the morphological information and the description of the state of the phases. In the porous polymeric systems with high surface area, xenon can diffuse through the pores and can reach rapidly the amorphous phases of the material. The xenon signals ranging from 210 to 230 ppm provide information on the explored amorphous phases. The gas uptake is inhibited in the glassy state while gas absorption becomes progressively higher on increasing the temperature beyond glass transition. The high sensitivity of the method could detect even minor amounts of xenon uptake, thus determining, with notable accuracy, the onset of cooperative motions in pure phases and blends. We have established the existence of separate domains of polypropylene and EPR phases larger than 200 nm that, however, exchange xenon massively in a few hundred milliseconds as shown by 2D HP NMR experiments. Using this novel tool, it was possible to demonstrate in the PP/EPR blends that EPR rubber receives first the fresh hyperpolarized xenon and then exchanges xenon with the PP phase.

In general, our experiments based on the recognition of the phases and transport phenomena define a hierachical structure of microphases able to interact with the gas phase. The complex architecture within the particles could explain both the accessibility of the monomers over preformed particles at successive polymerization steps and the high-impact properties of the PP/EPR intimate blends obtained by this preparation route. The unprecedented application of high sensitivity HP ^{129}Xe NMR to a rubbery polymeric material is promising for the study of complex polymeric architectures and extended polymeric interfaces.

Acknowledgment. The authors of this paper wish to thank G. Morini and F. Piemontesi from Basell for providing the samples and Prof. E. Grilli for helpful discussions about the optical system. The Ministry of Research and University and CARIPLO Foundation are acknowledged for financial support.

Supporting Information Available: Pictures of PP based particles, DSC traces of the samples, ^{13}C MAS NMR spectra, X-ray diffraction data, 2D EXSY NMR spectrum, CF−HP ^{129}Xe NMR spectra of pure EPR, and a table with chemical shift and peak intensity of xenon dissolved in PP and EPR phases at room temperature. This material is available free of charge via the Internet at http://pubs.acs.org.

CM060499H